JETIR.ORG ISSN: 2349-5162 | ESTD Year : 2014 | Monthly Issue
JOURNAL OF EMERGING TECHNOLOGIES AND INNOVATIVE RESEARCH (JETIR)
An International Scholarly Open Access, Peer-reviewed, Refereed Journal

GRID TIED SINGLE PHASE PHOTOVOLTAIC SYSTEMS WITH FUZZY LOGIC CONTROLLER

YENDLURI SUNIL KUMAR
MTech Student
Department of Electrical Engineering
Andhra University College of Engineering (A)
Visakhapatnam, AndhraPradesh,India.

Dr. G.V.SIVA KRISHNA RAO
Professor
Department of Electrical Engineering,
Andhra University College of Engineering (A) Visakhapatnam.
AndhraPradesh,India

ABSTRACT

Grid-connected photovoltaic (PV) systems are increasingly attracting the attention of industry and academia as a means of providing an alternative to conventional fossil-fuel generation. In grid-connected PV systems, a key consideration is the design and operation of power converters and how to achieve high efficiency for different power configurations.

The modelling, design, and control of a solar supply (PVS) for a single-phase grid system are presented in this work. A step-up converter (SUC) is used in the two-stage conversion process between the photovoltaic panel and the voltage source converter's dc bus (VSC). An SUC switching method based on fuzzy logic control (FLC) is developed for the maximum power tracking (MPT) at PVS terminals. Utilizing a modified multilayer fifth-order generalised integrator (mMLFOGI), a band-pass filter (BPF) is created to estimate the synchronising grid supply signals for the control of VSC. Under grid disturbances such dc offsets, frequency fluctuations, voltage sag, swell, and harmonics, the mMLFOGI based BPF provides appropriate synchronisation of VSC. These suggested control strategies are modelled in MATLAB.

Key words **– Fuzzy logic, maximum power tracking (MPT), modified multilayer fifth-order generalized integrator (mMLFOGI), photovoltaic supply (PVS), voltage source converter(VSC).**

I INTRODUCTION

In order to reduce the generation from fossil fuel-driven sources, there has been an increase in the trends of integrating renewable energy at the grid system's distribution level. Photovoltaic (PV) systems powered by solar energy are often deployed at the distribution end. The varieties of grid system integration are single-phase or three-phase in nature, depending on the rating of PV installations. Voltage source converters (VSCs), which are typically utilised between the PV panel output and the grid system to convert dc to ac power, are used because PV panels provide dc electricity. The synchronisation of VSC with grid supply must be done correctly and in accordance with the rules established by national standards. When the grid is experiencing disruptions.

The photovoltaic supply system's (PVS) VSC is typically managed to control the injection of active and reactive power into the grid system and the enhancement of power quality at the point of common coupling (PCC). The literature contains a wide variety of additional techniques for reaching these control goals. However, the majority of them struggle to operate effectively when the grid is disrupted. According to Song et al., the deadbeat control has a large control bandwidth and a good dynamic response, but it is also very sensitive to system characteristics and unable to handle steady-state errors. For maximum power tracking, Fortunato et alin .'s one cycle control (OCC) only needs two sensors as opposed to four (MPT). However, OCC's stability in VSC's inverting mode of operation is debatable. VSC should synchronise under different grid disturbances, such as dc offsets, frequency fluctuations, voltage sag, swell, and harmonics, to improve the power quality and stability. By removing a unit template of fundamental voltage, the VSC is brought into synchronisation with the grid supply. Utilizing an orthogonal signal generator, it is obtained (OSG).

The authors have provided a performance comparison of OSG methods for extracting unit templates. Using a second-order generalised integrator (SOGI), modified-second-order generalised integrator (M-SOGI), mixed third-order and second-order

generalised integrator (MTSOGI), and new modified SOGI (mSOGI) structure, a band-pass filter (BPF) has been reported in the literature for synchronising the VSC. The SOGI, which has a straightforward design, is frequently used to synchronise the VSC with grid supply. However, when there is a dc offset in the grid voltage, the SOGI performs poorly and the synchronising signals lag behind the core component of the grid voltage. Both an M-SOGI and an MTSOGI have been proposed as solutions to this issue. However, when harmonics are present, both of these techniques perform less well. A report of the mSOGI has been made.
Under diverse grid disturbances, the BPF employing mSOGI and MLFOGI is particularly effective in obtaining a fundamental unit template. In mSOGI, the parameters for the various BPF layers are determined using a pole placement approach, whereas in MLFOGI, they are directly obtained using a characteristic equation. To make it simpler for real-time implementation, the transfer function in MLFOGI for the various layers of harmonic extraction must be simplified. In order to synchronise the VSC of PVS with the grid system, this study uses a modified multilayer fifth-order generalised integrator (mMLFOGI) based BPF with a simplified transfer function for the third and fifth harmonic extraction layers.
The modelling, design, and control of a two-stage PVS conversion for a single-phase grid system are presented in this paper. Between a PV panel and a dc bus, a step-up converter, or SUC, is utilised. To get the most power out of a PV panel, many control strategies based on a classical method, a search algorithm, and artificial intelligence have been reported. P&O (perturb and observe) and IC (incremental conductance) are two techniques that are frequently utilised in the classical method. They are both straightforward and less complicated. These methods do, however, function slowly and fluctuate in output power. Modified (P&O) and modified IC processes have smaller step sizes. Power tracking is sluggish as a result, though. Optimization-based search techniques include the JAYA algorithm, human psychological optimization, and particle swarm optimization. algorithm. Applications for tracking your whereabouts globally employ these techniques. But their digital implementations need a lot of memory. Up to a certain point, MPT techniques based on neural networks (NNs) and fuzzy logic control (FLC) have also been tried for PVS systems. For the purpose of training neurons, the NN-based MPT algorithm needs a significant amount of sample data. In comparison to NN, the FLC-based technique is simpler and easier to apply. The SUC is switched using the FLC-based MPT control in this work.
The main contributions of this paper :
→It is possible to synchronise the VSC in dynamic conditions with the improved tracking capability of mMLFOGI-based BPF.
→For SPV supply that is integrated with the grid system for high-energy extraction, an FLC-based MPT algorithm is developed in real time.

II PV ARRAY

Photovoltaic Effect

Photovoltaic (PV) is a method of generating electrical power by converting solar radiation into direct current electricity using semiconductors that exhibit the photovoltaic effect. Photovoltaic power generation employs solar panels comprising a number of cells containing a photovoltaic material. Materials presently used for photovoltaic include mono crystalline silicon, polycrystalline silicon, amorphous silicon, cadmium telluride, and copper indium selenide/sulfide. Due to the growing demand for renewable energy sources, the manufacturing of solar cells and photovoltaic arrays has advanced considerably in recent years. The photovoltaic effect is the generation of a voltage (or a corresponding electric current) in a material upon exposure to light. Though the photovoltaic effect is directly related to the photoelectric effect, the two processes are different and should be distinguished. In the photoelectric effect, electrons are ejected from a material's surface upon exposure to radiation of sufficient energy.

The photovoltaic effect is different-in that the generated electrons are transferred between different bands (i.e. from the valence to conduction bands) within the material, resulting in the buildup of a voltage between two electrodes. In most photovoltaic applications the radiation is sunlight and for this reason, the devices are known as solar cells. In the case of a p-n junction solar cell, illumination of the material results in the generation of an electric current as excited electrons and the remaining holes are swept in different directions by the built-in electric field of the depletion region. The photovoltaic effect was first observed by Alexandre-Edmond Becquerel in 1839.

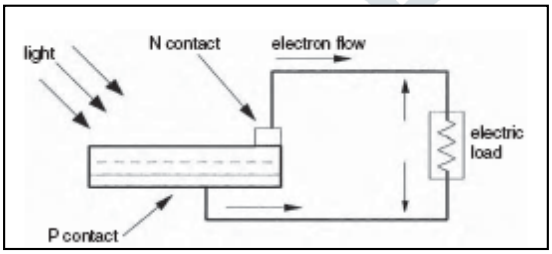

Fig 1: PV Effect converts the photon energy into a voltage across the PN junction

As of October 2010, the largest photovoltaic (PV) power plants in the world are the Sarnia Photovoltaic Power Plant (Canada, 80 MW), Olmedilla Photovoltaic Park (Spain, 60 MW), Strasskirchen Solar Park (Germany, 54 MW), Liberace Photovoltaic Park (Germany, MW), the Puertollano Photovoltaic Park (Spain, 50 MW), the Moura photovoltaic power station (Portugal, 46 MW), and Waldpolenz Solar Park (Germany, 40 MW).

Main Operation:The solar cell works in three steps:Photons in sunlight hit the solar panel and are absorbed by semiconducting materials, such as silicon.Electrons (negatively charged) are knocked loose from their atoms, allowing them to flow through the material to produce electricity. Due to the special composition of solar cells, the electrons are only allowed to move in a single direction.An array of solar cells converts solar energy into a usable amount of direct current (DC) electricity.

Equivalent Circuit:

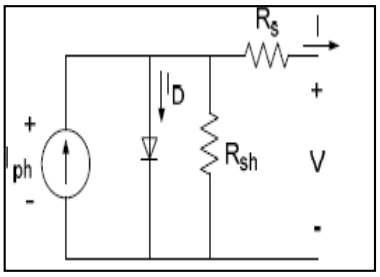

Fig 2.4: PV cell equivalent circuit

The complex physics of the PV cell can be represented by the equivalent electrical circuit. The circuit parameters are as follows. The current at the output terminals is equal to the light-generated current I_{ph}, less the diode current I_D, and the shunt-leakage current I_{sh}. The series resistance R_s represents the internal resistance to the current flow, and depends on the PN junction depth, impurities, and contact resistance. The shunt resistance R_{sh} is inversely related to the leakage current to the ground. In an ideal PV cell, $R_s = 0\Omega$ (no series loss), and $R_{sh} = \infty$(no leakage to ground).In a typical high-quality silicon cell, Rs varies from 0.05 to 0.10 Ωand R_{sh} from 200 to 300 Ω. The PV conversion efficiency is sensitive to small variations in Rs, but is insensitive to variations in R_{sh}. A small increase in Rs can decrease the PV output significantly. In the equivalent circuit, the current delivered to the external load equals the current I_L generated by the illumination, less the diode current Id and the shunt leakage current I_{sh}. The open-circuit voltage $V_{oc}$of the cell is obtained when the load current is zero ,i.e.,when

I= 0, and is given by the following:

$$V_{oc} = V + IR_{sh}$$

The shunt resistance (R_{sh}) is very large and the series resistance (Rs) is very small. Therefore, it is common to neglect these resistances in order to simplify the solar cell model. The resultant deal voltage-current characteristic of a photovoltaic cell is given by the relation below and illustrated by the figure above.

$$I = I_{ph} - I_D$$

$$I = I_{ph} - I_0\left[\exp\left(\frac{q(V+R_sI)}{Ak_BT}\right) - 1\right] - \frac{V+R_sI}{R_{sh}}$$

Where,

I_{ph} = photocurrent, I_D = diode current, I_0 = saturation current, A = deality factor, q = electronic charge $1.6x10^{-9}$,

k_B = Boltzmann's gas constant ($1.38x10^{-23}$), T = cell temperature, R_s = series resistance, R_{sh} = shunt resistance, I = cell current,

V = cell voltage

The power output of a solar cell s given by

$$P_{PV} = V_{PV} * {}_{PV}$$

Where,

I_{PV}= Output current of solar cell (A), V_{PV}= Solar cell operating voltage (V), P_{PV} =Output power of solar cell (W).

The power-voltage (P-V) characteristics of a photovoltaic module operating at a standard irradiance of 1000 W/m^2 and temperature of 25ºC s shown below.

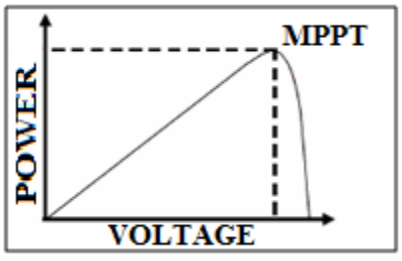

Fig 5: Power-Voltage (PV) Characteristic of a Photovoltaic Module

It can be seen from the characteristics, that there is a unique point in the characteristics at which the photovoltaic power is maximum. This point is termed the maximum power point (MPP). The power corresponding to this point s termed as power at maximum power point (P_{mpp}) and the voltage as the voltage at maximum power point (V_{mpp}). Due to high cost of solar cells, t must be ensured that the photovoltaic array operates at all time to provide maximum power output. Hence a maximum power point tracker must be used to track the maximum power of the system. This is commonly known as maximum power point tracking (MPPT).

Now if the irradiance level of the photovoltaic system is changed from the standard 1000 W/m^2 to say 600 W/m^2 or 400 W/m^2 then the P-V characteristic will change as shown in the figure below.

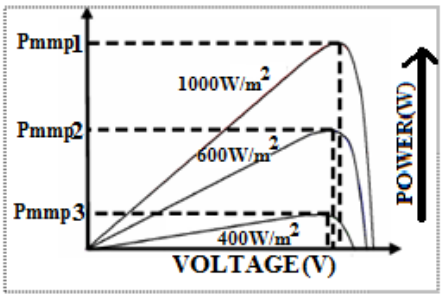

Fig 6: Variation of P-V Characteristics of Photovoltaic Module

The above graph shows that, the maximum power of the PV system also reduces accordingly. The maximum power point tracker must now track the new maximum power point for the changed irradiance level.

When multiple PV cell modules are put together, they can form an arrangement called an array or array field. In general, the larger area of a module or array, The more electricity that will be produced. Photovoltaic modules and arrays produce direct current (dc) electricity. They can be connected in both series and parallel electrical arrangements to produce any required voltage and current combination.

III DC-DC CONVERTER

DC-DC CONVERTER

A basic DC-DC converter consists of energy transferred from load to the energy storage devices like inductors or capacitor through switches like a transistor or a diode. They can be used as linear voltage regulators or switched mode regulators. In a linear voltage regulator, the base voltage of a transistor is driven by a control circuit to obtain the desired output voltages. In a switched mode regulator, transistor is used as a switch. In a step down converter or a buck converter, when switch is closed, the inductor allows current to flow to the load and when the switch is opened, the inductor supplies the stored energy to the load.

3 Categories of DC-to-DC Converter:

- Buck converters
- Boost converters
- Buck boost converters

❖**Without using the Boost Converter:**

In semiconductor switching devices, the Linear regulated circuits (DC power regulated circuits) access voltage from the unregulated input supply (AC power supply) and due to this there is a power loss. The power loss is proportional to the voltage drop.

❖**Using the Boost Converters:**

In switching devices, the converters converts the unregulated AC or DC input voltage to regulated DC output voltage.

DC-DC Boost converter

The configuration of the boost converter is as shown in the figure below.

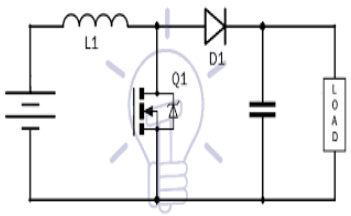

Fig.1 DC-DC boost converter.

Working:

A boost converter (step-up converter), as its name suggest step up the input DC voltage value and provides at output. This converter contains mostly a diode, a transistor as switches and at least one energy storage element. Capacitors are usually added to output so as to perform the function of removing output voltage ripple and sometimes inductors a

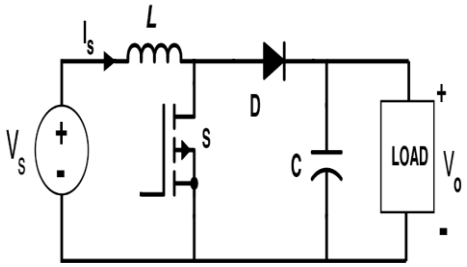

Fig 3: **Basic boost circuit**.

Its operation is generally of two separate states, During the ON period, switch is made to close its

- contact is which results in increase of inductor current. During the OFF period, switch is made to open
- Thus the only path for inductor current to flow through the fly-back diode 'D' and the parallel combination of capacitor and load. This enables capacitor to transfer energy gained by it during ON period

Basic Operation: The boost converter is a medium of power transmission to perform energy absorption and injection from solar panel to grid-tied inverter. The process of energy absorption and injection in boost converter is performed by a combination of four components which are inductor, electronic switch, diode and output capacitor. The connection of a boost converter is shown in Figure . The process of energy absorption and injection will constitute a switching cycle [5]. In other word, the average output voltage is controlled by the switching on and off time duration. At constant switching frequency, adjusting the on and off duration of the switch is called pulse-width-modulation (PWM) switching. The switching duty cycle, k is defined as the ratio of the on duration to the switching time period. The energy absorption and injection with the relative length of switching period will operate the converter in two different modes known as continuous conduction mode (CCM) and discontinuous conduction mode.

A. CONTINUOUS-CONDUCTION MODE (CCM)

In CCM, power transfer is a two-step process. When the switch is ON, stored energy builds in the inductor. When the switch is OFF, energy transfers to the output through the diode. The switch current is a stepped saw tooth with a fixed steady-state ON time with some amount of ripple current superimposed. During the ON time of the switch, if we assume zero losses for the moment, the voltage across the inductor is approximately the input voltage; and the voltage across the rectifier is the capacitor, or output voltage. When the switch turns OFF, the energy stored in the inductor releases into the output through the rectifier. The voltage across the inductor is approximately the input-to-output voltage difference, and the voltage across the switch becomes approximately the output voltage (see Fig. 3). Important to any model is the understanding of the current in each of the relevant components in the power path. The mathematical construction of these currents helps to determine the magnitude and shapes of these currents.

With zero losses assumed, the inductor current's ON-time slope is

$$m_{I_{L(ON)}} = \frac{V_{IN}}{L}.$$

During the OFF time, the current will have a slope of

$$m_{I_{L(OFF)}} = \frac{V_{IN} - V_{OUT}}{L}.$$

If the V · s during the ON time of the switch is equated with the V · S during the OFF time of the switch,

$$\frac{V_{IN}}{L} \times D \times T_s = \frac{V_{IN} - V_{OUT}}{L} \times (1 - D) \times T_s.$$

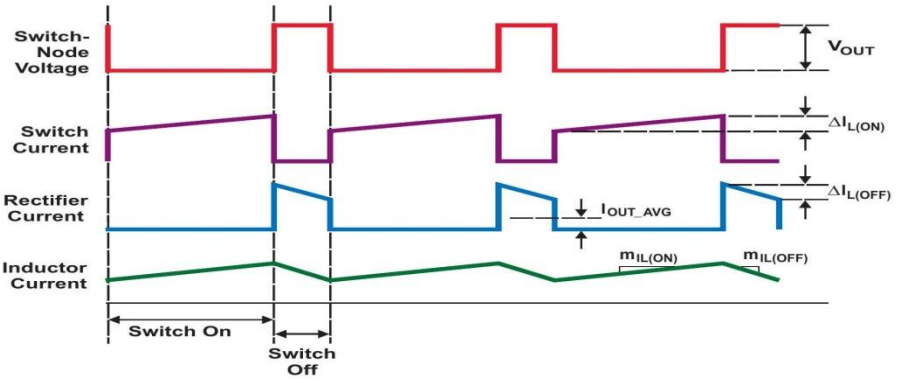

Fig. 4 .Representative CCM waveforms.

* For a glossary of variables. Solving for the switch duty cycle, D, results in

$$D_{CCM(\text{ ideal })} = 1 - \frac{V_{IN}}{V_{OUT}}.$$

Power-stage input and output losses that impact the duty cycle are shown in Fig. 4. The input losses include the inductor winding resistance (R_L), the switch MOSFET $R_{DS(ON)}$, and (in the case of a current-mode-controlled converter) a currentsense resistor (R_{ISENSE}). The output losses are represented by the output diode rectifier, D1.

If the loss elements of the power-stage components are included, the equation for the duty cycle in CCM is shown by Equation (5) below. Equation (5) holds true for CCM when the ripple current in the inductor is small relative to the average DC current. The equation is "close" when there is a high percentage of ripple current. Reassuringly, if the losses in Equation (5) reduce to zero, the equation simplifies to the ideal case.

B DISCONTINUOUS-CONDUCTION MODE (DCM)

In DCM, a switching cycle is composed of three intervals. The first two are the same as in CCM, where energy is stored in the inductor during the ON time of the switch, and transferred to the load during the OFF time of the switch. In DCM, however, all of the energy in the inductor transfers to the load during this second interval. The third interval begins when the energy in the inductor is depleted, and terminates at the end of the switching period the next time the switch turns on. During this third interval (the idle period in Fig. 5), the voltage across the inductor decays to zero, the voltage across the switch decays to the input voltage, and the input-to-output voltage differential is across the rectifier. There is essentially no current flowing in the power stage during this interval.

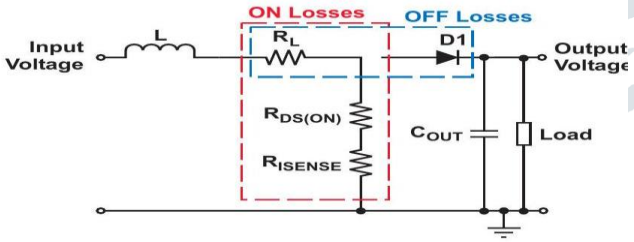

Fig. 5. Boost model with loss elements.

$$D_{CCM} = 1 - \frac{\left\{ V_{IN} + I \times (R_{DS(ON)} + R_{ISENSE}) + \sqrt{\left[V_{IN} + I_{OUT} \times (R_{DS(ON)} + R_{ISENSE}) \right]^2 - 4 I_{OUT} \times (R_{DS(ON)} + R_{ISENSE}) \times (V_{OUT} + V_d)} \right\}}{2(V_{OUT} + V_d)}$$

IV FUZZY LOGIC CONTROLLER

HOW DOES FUZZY LOGIC CONTROLLER WORK?

FLC requires some numerical parameters in order to operate such as what is considered significant error and significant rate-of-change-of-error, but exact values of these numbers are usually not critical unless very responsive performance is required in which case empirical tuning would determine them. For example, a simpletemperature control system could use a single temperature feedback sensor whose data is subtracted from the command signal to compute "error" and then time- differentiated to yield the error slope or rate-of-change-of-error, hereafter called "error-dot". The

"error-dot" might then have units of degs/min with a small error-dot being 5F/min and a large one being 15F/min.

These values don't have to be symmetrical and can be "tweaked" once the system is operating in order to optimize performance. Generally, FL is so forgiving that the system will probably work the first time without any tweaking.

It uses an imprecise but very descriptive language to deal with input data more like a human operator. It is very robust and forgiving of operator and data input and often works when first implemented with little or no tuning.

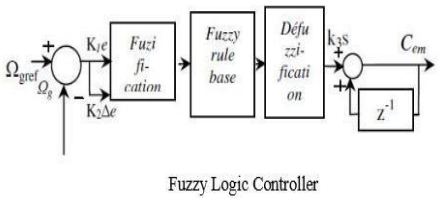

Fig: 1 fuzzy logic controller

THE OPERATION OF FUZZY CONTROLLER

In a fuzzy logic controller, the control action is determined from the evaluation of a' set of simple linguistic rules. The development of the rules requires a' thorough understanding of the process to be controlled, but it does not require a mathematical model of the system. The design of a fuzzy logic controller requires the choice of membership functions.

It consists of a number of Fuzzy If-Then rules that completely define the behavior of the system. These rules very much resemble the human thought process, thereby providing artificial intelligence to the system.

The error and change of error are used numerical variables from the real system. To convert these numerical variables into linguistic variables, the following seven fuzzy levels or sets are chosen as:

NB (negative big)

NM (negative medium)
NS (negative small)
ZE (zero)
PS (positive small)
PM (positive medium)
PB (positive big) and presented in input and output normalized membership functions.

Fuzzy logic controller consists of four parts they are:

1) FUZZIFICATION, 2)MEMBERSHIP FUNCTIONS, 3)FUZZY INFERENCE ENGINE, 4)DEFUZZIFICATION

V GRID WITH PV SYSTEM CONSIDERING FLC

PROPOSED PHOTO VOLTAIC SYSTEM :

The schematic diagram of proposed PVS for the single-phasegrid system is shown in Fig. 1. It consists of PV panel, an SUC,a single-phase self-commutated switches based H-bridge VSC, an interfacing inductor (L_{VSC}), a ripple absorption filter (RAF), solid-state circuit breaker (CB), and single-phase grid system. The input terminals of the SUC are connected to a PV panel and it transfers power to the dc bus of a VSC. A dc-bus capacitor isused at output of SUC to stabilize the voltage. The mid-point ofeach leg of the VSC and the grid supply is interfaced through the inductor (L_{VSC}). An RAF is employed at PCC to absorb noises due to the switching of VSC. The solid state CB is employed to connect/disconnect the PVS with the grid system for grid restoration and outage conditions.

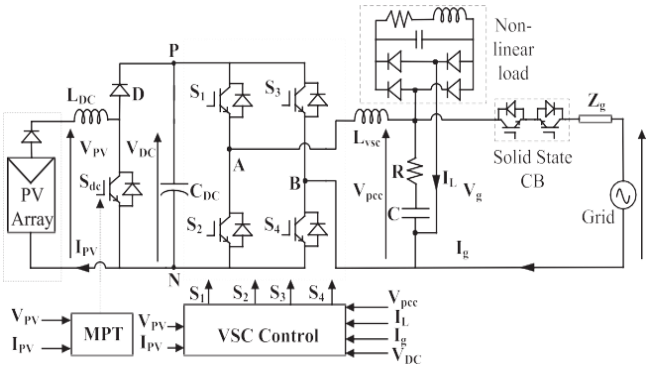

Fig. 1 : Schematic diagram of proposed single-phase photovoltaic supply.

The proposed PVS is designed for a small roof top for the rating of 640 W. Various sections of this system are designed as follows.

A. PV Panel

A 640 W PV panel with a peak output power at standard environmental conditions (1000 W/m^2 @25 °C) is selected. PV modules (CS5C-80 M) with 36 cells connected in series are selected to assemble the PV panel of the relevant size. The short-circuit current of a PV array is 4.97 A, and its open-circuit voltage is 21.8 V similarly, its MPT voltage and current are 17.5 V and 4.58 A, respectively. The power developed through the PV panel is obtained as

$$P_{\mathrm{PV}} = n_s n_p P_{\mathrm{m}} \eta_{\mathrm{mpt}} \quad (1)$$

where n_s and n_p are number of PV modules present in series and parallel combinations, respectively, P_m is developed powerthrough a single module, η_{mpt} is efficiency at maximum power

point. The PV modules connected in series are decided according to the desired PV voltage. n_s is selected eight to achieve voltage level of 140 V, and $n_p = 1$.

B. Inductor of SUC

The inductor of SUC is based on the PV panel voltage (V_{PV})and the dc-bus voltage (V_{DC}). The output voltage of SUC is 180 V in this case. The duty cycle (D) for SUC is given as

$$D = 1 - (V_{\mathrm{PV}}/V_{\mathrm{DC}}). \quad (2)$$

The value of "D" is obtained at minimum solar irradiation, i.e., 200 W/m^2, the PV panel voltage is 138 V, and the duty cycle is calculated as 0.24.

The inductor (L_{DC}) value is a function of PV panel voltage(V_{PV}), inductor ripple current Δi_{LDC}, D, and switching frequency (f_s) as

$$L_{\mathrm{DC}} = (V_{\mathrm{PV}} D)/(f_s \Delta I_{\mathrm{LDC}}). \quad (3)$$

The highest value of inductor is obtained at minimum solar irradiation, i.e., minimum PV panel current. The MPT current at 200 W/m^2 is 0.92 A and flows through the inductor L_{DC}. Forthe 0.2 p.u. of inductor ripple current, i.e., 0.92 A, switching frequency of 30 kHz, the value of L_{DC} is obtained as 6 Mh.

C. DC-Bus Capacitor

The value of dc-bus capacitor is determined as

$$C_{\mathrm{DC}} \geq P_{\mathrm{DC}}/(2\pi f_g V_{\mathrm{DC}} \Delta V_{\mathrm{DC}}) \quad (4)$$

where P_{DC} is power at dc bus, ΔV_{DC} is allowable ripple contents in voltage at dc bus. It is considered 10% of its nominal value.f_g is the supply frequency, i.e., 50 Hz. C_{DC} is calculated as 628 μF and it is considered 1000 μF in the simulation model and prototype.

D. Interfacing Inductor

The interfacing inductor is used in between ac supply terminals and mid-point of VSC to absorb the differences in instantaneous voltages. The value of ac interface inductor is givenas

$$L_{\mathrm{VSC}} = V_{\mathrm{DC}}/(8 f_{\mathrm{VSC}} \Delta I_{\mathrm{VSC}}) \quad (5)$$

where f_{VSC} is switching frequency of VSC, i.e., 10 kHz, the allowable ripple contents in inductor current is 5% of its nominal value. The value of inductor is estimated as 7.75 mH.

E. Ripple Absorption Filter

The switching noises are generated due to VSC. It causes distractions in quality of PCC voltages. An RAF is connected atthe PCC. The values of its element are obtained based on timeconstant of RAF. This time constant should be very much less than time period of carrier waveform [29] ($T_s = 1/f_{\mathrm{VSC}}$), i.e.,$RC \ T_s/10$, considering $RC = T_s/10$, and switching frequencyof 10 kHz, the values of R and C are obtained as 1 Ω and10 μF, respectively.

CONTROL OF SYSTEMS : Two sections are used to present the control of PVS for single-phase grid systems. The control of SUC is discussed in the first part. To get the most power possible out of the PV panel, the SUC is adjusted. The FLC method is used to transmit the most power possible from the PV panel to the DC bus of the VSC. The control of VSC is discussed in the section that follows. An mMLFOGI-based BPF is used to synchronise the VSC and transfer PV generated power into the grid supply and loads. The following is a presentation of the SUC control schemes.

A. Control of SUC

For MPT control, the FLC approach is implemented. The out- put of FLC is the change in duty cycle. The error E ($dP_{\mathrm{PV}}/dV_{\mathrm{PV}}$) and change in error ΔE are input to the FLC. The Mamdani's approach is used in designing the FLC. There are four steps, i.e., fuzzification of input variables into linguistic variables, aggre-gation using output rules, rules evolutions, and defuzzification for converting linguistic to real values of output. The E and $\Delta E$are evaluated in each sample time as follows:

$$E(k) = \{P(k) - P(k-1)\}/\{V(k) - V(k-1)\} \quad (6)$$

$$\Delta E(k) = E(k) - E(k-1). \quad (7)$$

The triangular membership function is used for input vari- ables expressed as positive big (PB), positive small (PS) zero (ZE), negative small (NS), and negative big (NB), as shown inFig. 2. Similarly five membership functions are used for outputvariables expressed as PB, PS, ZE, NS, and NB, respectively. The FLC rules are designed

The block diagram for implementation of FLC-based MPT is given in Fig. 3.

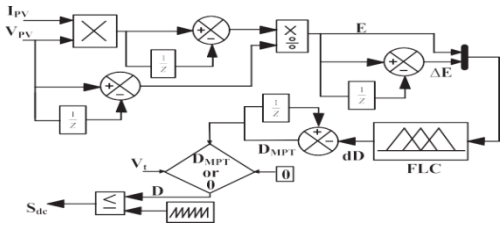

Fig. 5.2. Block diagram of SUC control

In Fig. 3, switching signal for SUC is generated from FLC block. However, it is released to switch only when the grid supply is available. If the grid supply fails or deviates from nominal conditions, solid state CB opens and switching signals to switch is blocked immediately. The logic expression for SUCcontrol is obtained as

```
function D = fnc(Vt, DMPT)
if Vt >= 0.8*110*sqrt(2) && Vt <= 1.2*110*sqrt(2);
D=DMPT;
else
D=0;
end
end
```

where V_t is amplitude of voltage at PCC.

Results and discussions from simulations

In MATLAB Simulink, a double-stage PVS system connected to a single-phase grid is modelled.

The PVS system is modelled after a 640 W PV panel. The performance is seen in various grid supply grid disturbance and irradiation profiles. Performance is tracked using the solar irradiations [G(t)], voltage (VPV), and current (IPV) at PV panel terminals, power (PPV) at PV panel, voltage (VDC) at DC bus, supply voltage (Vg), supply current (Ig), load current (IL), power injection (Pg) at grid terminals, load power (PL), fundamental component of PCC voltage (Vpcc), and unit template (ut). The Appendix contains a list of the simulation model's input parameters.

Performance During Grid Disruption:

performance of a single-phase grid-tied PVS system when the grid supply is disrupted. These outcomes were attained with the use of VPV, IPV, VDC, Vg, V, V, ut, Ig, PPV, and Pg. Voltage swell, sag, and dc-offset are a few of the disturbances seen in Vg. There is a 20% voltage swell visible in Vg between 2.2 and 2.4 s. Pg, however, remains constant and follows MPT from a PV panel. Nominal supply voltage is shown at PCC at 2.4 s. 20% voltage sag is induced into Vg between 2.8 and 3.2 s, which causes current to be injected into the grid to increase in order to maintain constant Pg. A 15 voltage dc-offset is injected into the Vg at 2.8 seconds. One observes that even The synchronisation unit template is correct and unaffected even under such extreme supply voltage variations. The measured rated grid voltage and grid injected current rise from 2.4 to 2.8 seconds. 20% voltage sag is put into the grid at 2.8 seconds, and current pumped into the grid increases once again. 15 dc-offset voltages are added to the grid voltage at 2.8 seconds.

Results are shown in Fig. 5.4 when the grid supply frequency is changed and third- and fifth-harmonic presence is present. The rated grid frequency is lowered to 48 Hz between 3.8 and 4 seconds. Third harmonics having a magnitude of 10% of the rated voltage are added to the ac supply voltage at 4 seconds. Fifth harmonics with a magnitude of 10% of the rated voltage are added to the grid voltage at 4.4 s, and third and fifth order harmonics with magnitudes of 10% of the grid voltage are added at 4.8 s. The grid current is also kept sinusoidal under such grid voltage perturbations, and VSC continues to be in synchronism with the grid supply.

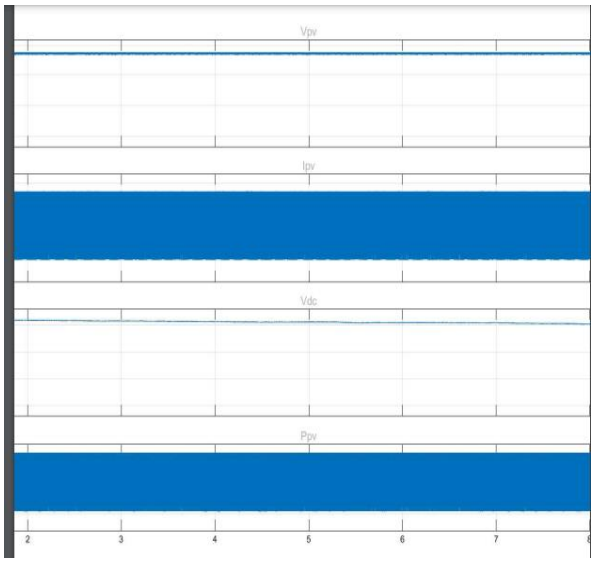

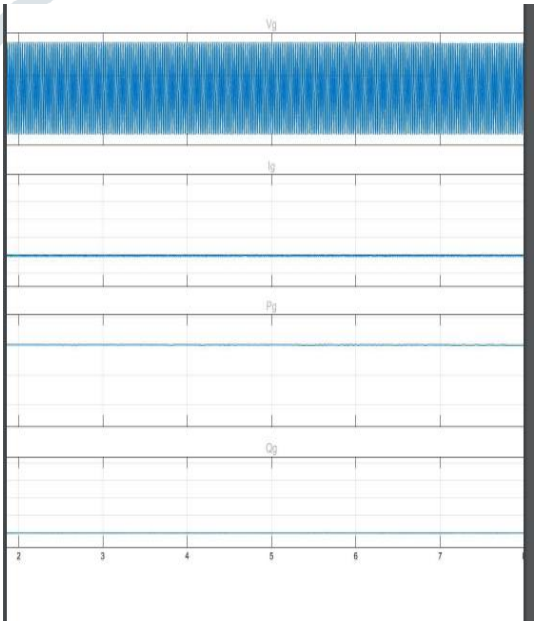

Fig 5.3 Performance of PVS system under voltage sag, swell, and dc offset in grid supply.
supply voltage of grid.

fig .4 Performance of PVS system under frequency variations, third and fifth harmonics in .

VI CONCLUSION

For the synchronisation of VSC for PV power generation integrated with the single-phase grid system, the mMLFOGI-based BPF has been presented. Utilizing SUC, the FLC has been utilised to extract the most electricity possible from solar panels. Even under grid-polluted conditions such voltage sag, swell, harmonics, and frequency variation, the mMLFOGI-based BPF has shown valuable in extracting fundamental grid voltage components for synchronisation with the grid supply. Under steady-state conditions, the FLC-based MPT technique guarantees quick dynamic reaction and low oscillation in PV voltage and current. Additionally, it makes for improved energy extraction. The effectiveness of the PVS system has been demonstrated through extensive simulation simulations.

VII REFERENCES

[1] S. Pradhan, B. Singh, and B. K. Panigrahi, "A digital disturbance esti- mator (DDE) for multiobjective grid connected solar PV based distributed generating system," *IEEE Trans. Ind. Appl.*, vol. 54, no. 5, pp. 5318–5330, Sep./Oct. 2018.

[2] W. S. Song, J. P. Ma, L. Zhou, and X. Y. Feng, "Deadbeat predictive power control of single-phase three-level neutral-point-clamped converters using space-vector modulation for electric railway traction," *IEEE Trans. Power Electron.*, vol. 31, no. 1, pp. 721–732, Jan. 2016.

[3] M. Fortunato, A. Giustiniani, G. Petrone, G. Spagnuolo, and M. Vitelli, "Maximum power point tracking in a one cycle controlled single stage photovoltaic inverter," *IEEE Trans. Ind. Electron.*, vol. 55, no. 7, pp. 2684–2693, Jul. 2008.

[4] E. S. Sreeraj, K. Chatterjee, and S. Bandyopadhyay, "One cycle-controlled single-stage single-phase voltage-sensor less grid connected PV sys- tem," *IEEE Trans. Ind. Electron.* vol. 60, no. 3, pp. 1216–1224, Mar. 2013.

[5] D. V. Ghodke, K. Chatterjee, and B. G. Fernandes, "Modified one-cycle controlled bidirectional high-power-factor AC-to-DC converter," *IEEE Trans. Ind. Electron.* vol. 55, no. 6, pp. 2459–2472, Jun. 2008.

[6] N. Mahmud, A. Zahedi, and A. Mahmud, "A cooperative operation of novel PV inverter control scheme and storage energy management system based on ANFIS for voltage regulation of grid-tied PV system," *IEEE Trans. Ind. Informat.*, vol. 13, no. 5, pp. 2657–2668, Oct. 2017.

[7] P. E. Kakosimos, A. G. Kladas, and S. N. Manias, "Fast photovoltaic system voltage- or current-oriented MPPT employing a predictive digital current-controlled converter," *IEEE Trans. Ind. Electron.*, vol. 60, no. 12, pp. 5673–5685, Dec. 2013.

[8] S. Yu, L. Zhang, H. H. C. Iu, T. Fernando, and K. P. Wong, "A DSE-based power system frequency restoration strategy for PV-Integrated power sys- tems considering solar irradiance variations," *IEEE Trans. Ind. Informat.*, vol. 13, no. 5, pp. 2511–2518, Oct. 2017.

[9] Y. Han, M. Luo, X. Zhao, J. M. Guerrero, and L. Xu, "Comparative per- formance evaluation of orthogonal-signal generators-based single-phase PLL algorithms-A survey," *IEEE Trans Power Electron* ., vol. 31, no. 5, pp. 3932–3943, May 2016.

[10] S. Golestan, J. M. Guerrero, F. Musavi, and J. C. Vasquez, "Single-phase frequency locked loops: Comprehensive review," *IEEE Trans Power Elec-tron*., vol. 34, no. 12, pp. 11791–11812, Dec. 2019.

[11] P. Rodríguez, A. Luna, I. Etxeberria, J. R. Hermoso, and R. Teodorescu, "Multiple second order generalized integrators for harmonic synchroniza- tion of power converters," in *Proc. IEEE Energy Convers. Congr. Expo.*, Terrassa, Spain, Sep. 2009, pp. 2239–2246.

[12] M. Xie, H. Wen, C. Zhu, and Y. Yang, "DC offset rejection improvement in single-phase SOGI-PLL algorithms: Methods review and experimental evaluation," *IEEE Access*, vol. 5, pp. 12810–12819, 2017.

[13] C. Zhang, X. Zhao, X. Wang, X. Chai, Z. Zhang, and X. Guo, "A Grid synchronization PLL method based on mixed second- and third-order gen- eralized integrator for DC offset elimination and frequency adaptability," *IEEE J. Emerg. Sel. Topics Power Electron.* vol. 6, no. 3, pp. 1517–1526, Sep. 2018.

[14] C. M. Hackl and M. Landerer, "Modified second-order generalized inte- grators with modified frequency locked loop for fast harmonics estimation of distorted single-phase signals," *IEEE Trans Power Electron*., vol. 35, no. 3, pp. 3298–3309, Mar. 2020.

[15] N. Kumar, I. Hussain, B. Singh, and B. K. Panigrahi, "Implementation of multilayer fifth-order generalized integrator-based adaptive control for grid-tied solar PV energy conversion system," *IEEE Trans. Ind. Informat.*, vol. 14, no. 7, pp. 2857–2868, Jul. 2018.

[16] P. K. Pardhi, S. K. Sharma, and A. Chandra, "Control of single phase solar photovoltaic supply system," in *Proc. IEEE Ind. Appl. Soc. Annu. Meeting*, Baltimore, MD, USA, 2019, pp. 1–14.

[17] M. Killi and S. Samanta, "Modified perturb and observe MPPT algorithm for drift avoidance in photovoltaic systems," *IEEE Trans. Ind. Electron.*, vol. 62, no. 9, pp. 5549–5559, Sep. 2015.

[18] D. Sera, L. Mathe, T. Kerekes, S. V. Spataru, and R. Teodorescu, "On the perturb-and-observe and incremental conductance MPPT methods for PV systems," *IEEE J. Photovolt.*, vol. 3, no. 3, pp. 1070–1078,